The Astrophysical Journal, 791:92 (9pp), 2014 August 20 doi:10.1088/0004-637X/791/2/92

WHITE DWARF COSMOCHRONOLOGY IN THE SOLAR NEIGHBORHOOD

P.-E. Tremblay[1,3], J. S. Kalirai[1,2], D. R. Soderblom[1], M. Cignoni[1], and J. Cummings[2]
[1] Space Telescope Science Institute, 3700 San Martin Drive, Baltimore, MD 21218, USA; tremblay@stsci.edu
[2] Center for Astrophysical Sciences, Johns Hopkins University, 3400 North Charles Street, Baltimore, MD 21218, USA
Received 2014 May 6; accepted 2014 June 19; published 2014 July 31

ABSTRACT

The study of the stellar formation history in the solar neighborhood is a powerful technique to recover information about the early stages and evolution of the Milky Way. We present a new method that consists of directly probing the formation history from the nearby stellar remnants. We rely on the volume complete sample of white dwarfs within 20 pc, where accurate cooling ages and masses have been determined. The well characterized initial–final mass relation is employed in order to recover the initial masses ($1 \lesssim M_{\rm initial}/M_{\odot} \lesssim 8$) and total ages for the local degenerate sample. We correct for moderate biases that are necessary to transform our results to a global stellar formation rate, which can be compared to similar studies based on the properties of main-sequence stars in the solar neighborhood. Our method provides precise formation rates for all ages except in very recent times, and the results suggest an enhanced formation rate for the solar neighborhood in the last 5 Gyr compared to the range $5 <$ Age (Gyr) < 10. Furthermore, the observed total age of $\sim$10 Gyr for the oldest white dwarfs in the local sample is consistent with the early seminal studies that have determined the age of the Galactic disk from stellar remnants. The main shortcoming of our study is the small size of the local white dwarf sample. However, the presented technique can be applied to larger samples in the future.

Key words: Galaxy: disk – Galaxy: evolution – Galaxy: stellar content – solar neighborhood – white dwarfs

Online-only material: color figures

1. INTRODUCTION

The detailed study of stars in the solar neighborhood allows for the calibration of stellar structure and evolution models. This can be done for instance with precise measurements of the effective temperature, luminosity, and metal abundance of local stars in order to compare with predicted isochrones, or by surveying binaries where the age and distance of all components are expected to be identical. One significant advantage of the local sample is the abundance of data and the feasibility of creating large volume complete samples. It is then possible to learn about the stellar formation history (SFH) and the initial mass function (IMF), in principle for different Galactic components, i.e., the thin disk, thick disk, and halo, if one is able to identify independently the populations from kinematics or metallicities. Various studies have been aimed at identifying the SFH of the disk, with different techniques, and often with conflicting results. The most common approach has been to invert the observed color–magnitude diagram into an SFH using stellar isochrones (Hernandez et al. 2000; Vergely et al. 2002; Cignoni et al. 2006). Another group of studies have been employing stellar activity in low-mass stars as an indicator of age (Soderblom et al. 1991; Rocha-Pinto et al. 2000; Fuchs et al. 2009). Other techniques to derive the SFH include empirical age versus metallicity relations (see, e.g., Reid et al. 2007) and the age distribution of nearby open clusters (de la Fuente Marcos & de la Fuente Marcos 2004).

Age determination for individual stars is difficult with any method (see the review of Soderblom 2010), especially for large ages where the stellar activity is small, the age versus metallicity relation is uncertain, and the age sensitivity of the color–magnitude diagram is greatly diminished except for a few evolved stars. Even for the SFH in the last 5 Gyr, studies find rates ranging from a nearly constant value (Rocha-Pinto et al. 2000; Reid et al. 2007) to a significantly peaked distribution with a maximum 3–5 Gyr ago (Vergely et al. 2002; Cignoni et al. 2006; Fuchs et al. 2009). In this work, we rely instead on local stellar remnants, which can be studied to derive very accurate masses and cooling ages.

The white dwarf luminosity function, defined as the number of stars as a function of their intrinsic luminosity, has been used as a tool to determine the age of the thin disk (Winget et al. 1987; Liebert et al. 1988; Leggett et al. 1998). Further studies have also revealed the white dwarf spatial density and integrated formation rates (Liebert et al. 2005; Harris et al. 2006; Limoges & Bergeron 2010). The luminosity function can also, in principle, provide information about the SFH (Diaz-Pinto et al. 1994), although it is difficult to extract this quantity because of the degeneracy between mass and age at constant luminosity. Rowell (2013) have demonstrated the possibility of recovering the SFH from an inversion of the luminosity function. Nevertheless, the observed luminosity functions are drawn from samples that are not volume complete, such as the Sloan Digital Sky Survey (SDSS; Harris et al. 2006), and complex corrections for completeness and contaminations have to be made.

On a different front, several works have been aimed at identifying a complete volume-limited sample of white dwarfs around the Sun. Holberg et al. (2002) was the first study dedicated to this sample, where they estimated at the time that within 20 pc, only 65% of the stellar remnants were known. The goal of achieving a complete volume sample was pursued by different studies (Holberg et al. 2008; Sion et al. 2009), and Giammichele et al. (2012) most recently presented a homogeneous review of the 20 pc sample with a consistent set of model atmospheres in order to improve the derived stellar parameters and distances. They examine the properties of 168

[3] Hubble Fellow.

potentially close white dwarfs, and by comparing the space number density of the 13 pc and 20 pc samples, they estimate that the latter is more than 90% complete.

In this work, we rely on the results of Giammichele et al. (2012, hereafter GB12) to study the SFH in the local neighborhood. The significant advantage of this sample is that the white dwarfs have precise distances, luminosities, masses, and cooling ages. This allows for a direct conversion of the remnant parameters to initial stellar parameters, employing the well studied initial–final mass relation calibrated from clusters and binaries (Kalirai et al. 2005; Catalán et al. 2008; Kalirai et al. 2008, 2009; Williams et al. 2009; Dobbie et al. 2012), and stellar isochrones for the main-sequence lifetime. While there are still biases in the derivation of the global SFH since not all stars have become white dwarfs, our technique does not involve the calculation of a luminosity function where some of the information is lost. We compare our results to previous studies, including those relying on main-sequence stars. The local white dwarf sample is still fairly small with only around one hundred objects, however the proposed technique can be used in future studies. For instance, *Gaia* is expected to identify a volume complete sample of degenerates up to ∼40 pc, including accurate individual distances and masses from parallaxes and photometry, and stellar population identifications from proper motions (Carrasco et al. 2014). In Section 2, we review the observed degenerate star sample. We follow in Section 3 with our derived SFH in the solar neighborhood. In Section 4, we characterize our uncertainties and compare our results to those obtained with other independent techniques and observations. The conclusion follows in Section 5.

2. WHITE DWARF SAMPLE

We rely directly on the white dwarf parameters and associated uncertainties derived in Table 2 of GB12. The atmospheric parameters were determined from a combination of photometric, spectroscopic, and parallax observations, and we refer to GB12 for a complete description of the sample and observations. In most cases, the photometric technique provided the best constraint on the fundamental parameters, where the combination of the photometric fluxes and parallaxes allowed for $T_{\rm eff}$, radius, and distance determinations. The total mass and cooling age were then derived employing the evolutionary models of Fontaine et al. (2001). These models have C/O cores (50/50 by mass fraction mixed uniformly) and assume thick hydrogen layers ($M_{\rm H}/M_{\rm total} = 10^{-4}$) for H-atmosphere white dwarfs and thin layers ($M_{\rm H}/M_{\rm total} = 10^{-10}$) for helium and mixed atmospheres. When possible, the Balmer lines in the spectra were also compared with model atmospheres to provide both $T_{\rm eff}$ and $\log g$ (Bergeron et al. 1992). The evolutionary models described above were then used to determine the radius, mass, luminosity, cooling age, and finally distance in combination with the observed magnitude.

The atmospheric parameters were derived using model atmospheres from Tremblay et al. (2011), Bergeron et al. (2011), and Dufour et al. (2005, 2007), for pure-hydrogen, pure-helium, and metal-rich (DQ, DZ) atmospheres, respectively. The pure-hydrogen atmospheres include the Lyα red wing opacity (Kowalski & Saumon 2006). In the meantime, a new grid of predicted spectra for pure-hydrogen atmospheres including a three-dimensional treatment of the convection has been published (Tremblay et al. 2013). However, GB12 (see Figure 16) have already included a correction to their spectroscopically determined atmospheric parameters based on early results from the three-dimensional simulations (Tremblay et al. 2011), and they suggested an empirical correction assuming that the high-mass bump seen in the larger SDSS sample is entirely due to shortcomings in the one-dimensional model atmospheres. The latest three-dimensional corrections from Tremblay et al. (2013) are fairly similar to the empirical correction used in GB12, despite the fact that the latter did not include a $T_{\rm eff}$ correction. Since we bin the data in 1 Gyr intervals in this work, it is a very good approximation to use directly the results of GB12.

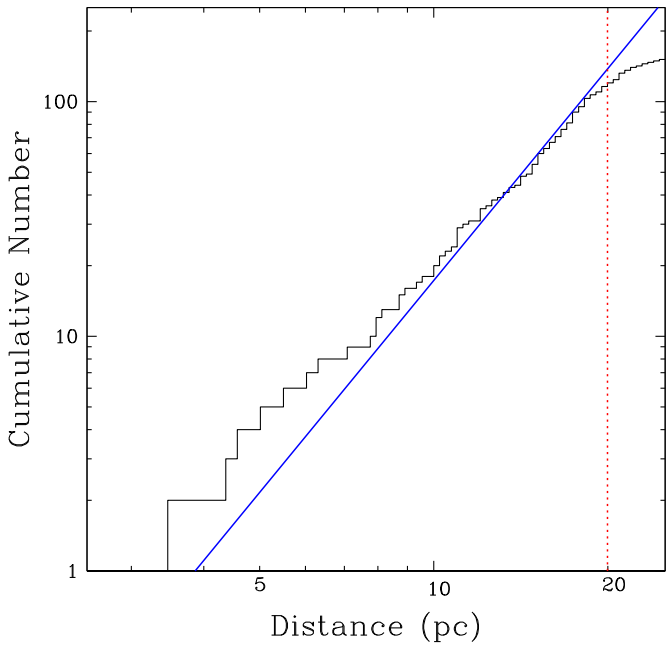

Figure 1. Number of white dwarfs as a function of distance (logarithm scales) for the local sample of GB12. The solid blue line represents the expected uniform distribution of stars for a volume complete sample normalized at the number of objects at 13 pc. The vertical dotted red line represents the 20 pc limit of this work.

(A color version of this figure is available in the online journal.)

In the following, we only keep objects with a derived distance smaller than 20 pc, for a total of 117 remnants. The sample does not include three white dwarfs in Sirius-like systems (Holberg et al. 2013) where the data on the degenerate counterpart is insufficient to derive the atmospheric parameters. Figure 1 reviews the 20 pc sample completeness by showing the cumulative number of objects as a function of distance. We compare with the expected +3 log–log slope for a complete sample, normalized at 13 pc assuming the sample is complete at this distance (Holberg et al. 2008). According to this normalization, the 20 pc sample is only 82% complete in contrast to the 90% value quoted in GB12. Their higher estimate is mostly because they increased the sample size by including objects that could lie within the uncertainties inside the 20 pc region, and also because they relied on the 13 pc number density from Holberg et al. (2008). The completeness already reaches 92% at 18 pc according to our results, hence we can review the integrity of the sample using both the 18 and 20 pc boundaries.

3. STELLAR FORMATION HISTORY

In order to study the SFH in the solar neighborhood, we need to recover the initial stellar parameters from the remnant properties. White dwarfs have been observed in different populations at solar metallicity to derive initial–final mass relations that are in relatively good agreement. We rely on the

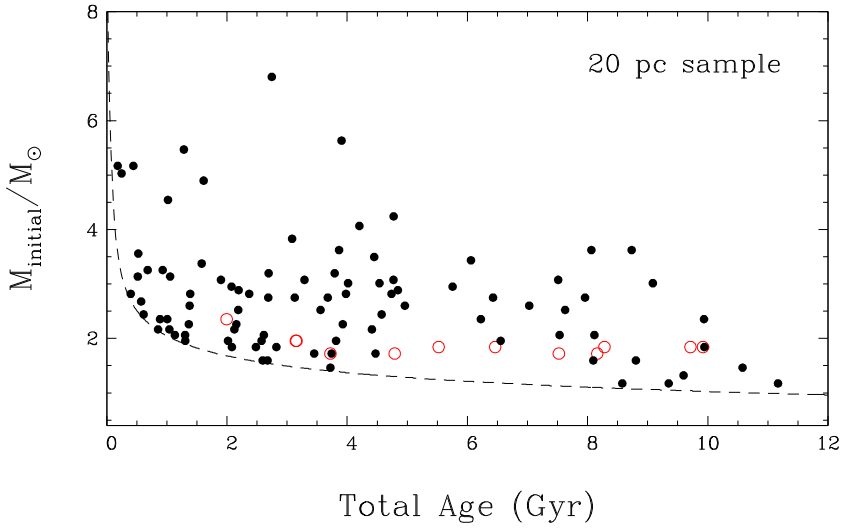

Figure 2. Initial mass distribution for the white dwarfs in the local 20 pc sample of GB12 as a function of total age. Masses were derived with the initial–final mass relation of Kalirai et al. (2008) and the total age is the sum of the white dwarf cooling time (Fontaine et al. 2001) and the main-sequence lifetime (Hurley et al. 2000). The dashed curve identifies where the total age is equal to the main-sequence lifetime, hence below which white dwarfs have not formed yet at present day. The remnants with a fixed $\log g = 8.0$ value are identified with open red circles.

(A color version of this figure is available in the online journal.)

prescription of Kalirai et al. (2008) who studied in particular the low-mass end of the initial–final mass relation in two open clusters.[4] The low-mass end is critical to study old stars in the solar neighborhood and difficult to observe due to the lack of close old clusters. The Kalirai et al. relation covers final masses in the range $0.53 \leqslant M_{\rm final}/M_{\odot} \leqslant 1.02$ corresponding to $0.8 \leqslant M_{\rm initial}/M_{\odot} \leqslant 6.5$. We use a third-order polynomial fit to the data.

We employ directly the white dwarf cooling ages derived in GB12 from the evolutionary models of Fontaine et al. (2001). The total age is the sum of the cooling age and the main-sequence lifetime from the evolution calculations of Hurley et al. (2000), assuming a solar metallicity, and the initial mass derived from the initial–final mass relation discussed above. Figure 2 presents the initial mass as a function of total age (lookback time) for the white dwarfs in the 20 pc sample. For 12 objects (red circles on the figure), no mass information is available, hence we assume the canonical $\log g = 8.0$ value to determine the initial stellar parameters. There are 13 objects, with a derived mean mass of $0.44 \pm 0.06\ M_{\odot}$, for which the total age would be significantly larger than the age of the universe. These objects are likely unresolved binaries (see GB12; Brown et al. 2011) and we exclude them from our analysis.

3.1. Biases

Figure 3 presents the number of white dwarfs in 1 Gyr age bins directly from the initial mass versus age distribution of Figure 2, which we define as the *raw* SFH (dashed red line). We also display in Figure 3 our best SFH estimate (filled black histogram) considering observational biases that we describe in the following sections. To begin, the total SFH is the sum of objects that are at present day white dwarfs, stars, and in much smaller number giants. In Section 3.1.1 we correct for the *missing main-sequence star bias*. The 20 pc sample is close to the central plane of the Galactic disk and populations with a small velocity dispersion in the vertical Galactic coordinate

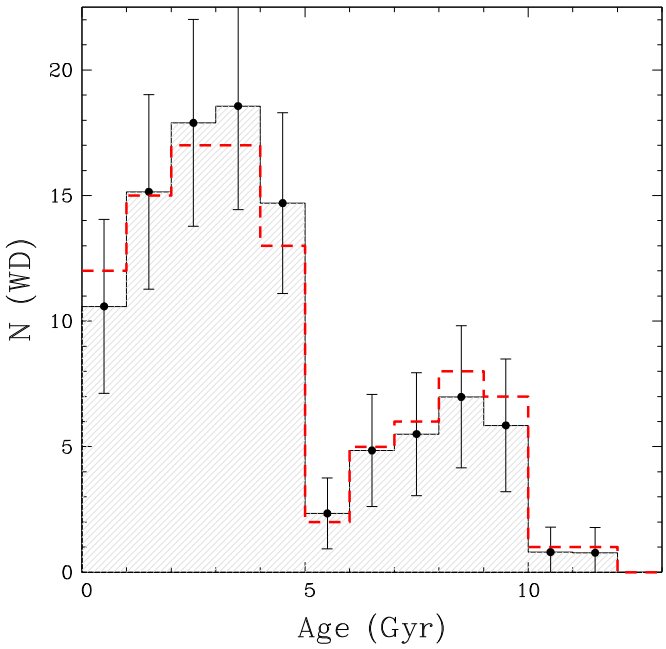

Figure 3. Number of white dwarfs in 1 Gyr total age bins (red dashed curve) from the data of Figure 2. The black filled histogram takes into account the biases due to the missing main-sequence stars (see Section 3.1.1) and the velocity dispersion σ_W in the Galactic coordinate W (see Section 3.1.2), and has been normalized for the same total number of stars. The error bars take into account number statistics uncertainties and are derived from the uncorrected number of white dwarfs.

(A color version of this figure is available in the online journal.)

are over represented. We correct for this *kinematic bias* in Section 3.1.2. Finally, Section 4.1 is devoted to other possible biases in order to highlight the uncertainties of our derivation.

3.1.1. Main-sequence

The main-sequence lifetime is larger than the lookback time in the initial mass versus age area below the dashed line in Figure 2. This region would be populated with H-burning stars that are

[4] We also use the more recent globular cluster constraints from Kalirai et al. (2009).

excluded from our sample. In order to derive the total SFH in the Galactic disk, we need to account for both main-sequence and degenerate stars. Calculating an absolute formation rate would be very difficult from white dwarfs alone since most of the stars are formed as M dwarfs, which are still on the main-sequence. In order to derive the relative formation rate, it is unnecessary to count all local stars, but we still have to account for the change, as a function of lookback time, of the ratio in number between white dwarfs and main-sequence stars in the present day population.

Figure 2 demonstrates that the separation between the white dwarf and stellar content of the Galaxy is fairly similar as a function of age. This is ensured by the rapid variation of the main-sequence lifetime as a function of initial mass. One exception is for the last Gyr bin where only stars born much more massive than the Sun became white dwarfs. To evaluate this bias, we computed the ratio of stars, assuming a Salpeter (1955) IMF, below and above the threshold between a present day white dwarf and a main-sequence star (dashed line in Figure 2). This ratio $B_{\rm MS-WD}$ is defined as

$$B_{\rm MS-WD} = \frac{\int_{M_0}^{M_{\rm lim}} M^{-2.35} dM}{\int_{M_{\rm lim}}^{M_1} M^{-2.35} dM}, \quad (1)$$

where

$$M_{\rm lim} = M(t_{\rm lookback} = t_{\rm main-sequence\ lifetime}), \quad (2)$$

while M_0 and M_1 are some arbitrary small and large masses outside of the $M_{\rm lim}$ range surveyed by our study. Values of M_0 and M_1 do not matter since we are only interested in the relative SFH. The obtained correction $B_{\rm MS-WD}$ is simply multiplied by the number of stars in each age bin and the full distribution is then re-normalized to the actual number of white dwarfs. Figure 4 (top panel) shows the effect of this bias alone in comparison to the raw distribution. The strongest effect is for ages below 1 Gyr, where the steepness of the IMF allows for few white dwarfs to be formed compared to larger ages.

In principle, it would be possible to compute the average IMF, i.e., integrated over all ages, directly from the results of the local white dwarf sample in Figure 2. However, the small size of the sample and properties of the IMF imply that only a small number of objects have masses 1σ higher than the average, and it is likely that the $\sim$15% missing white dwarfs in the sample are fainter hence more massive than the average. GB12 also suggest that the most massive objects may be the result of mergers. Therefore, we refrain from using the observed IMF, although we note that it is consistent with a fairly bottom-heavy IMF, with a power-law as much as 1 dex steeper than the Salpeter relation. This result is compatible with the lack of massive white dwarfs in the Hyades, just outside the 20 pc sample, considering a Salpeter IMF (Williams 2004; Tremblay et al. 2012). On the other hand, it is at odds with the Salpeter-like relation observed, on average, in nearby clusters (see, e.g., Weisz et al. 2013). We hope that larger and more complete white dwarf samples will be able to use the observed IMF in a consistent way to derive the SFH.

3.1.2. Kinematics

In this section we correct the SFH for kinematics. We have compiled the proper motions for the local sample (Sion et al. 2009, 2014) and Figure 5 demonstrates a tangential velocity ($v_{\rm tan}$) versus age relation, where the velocity was computed

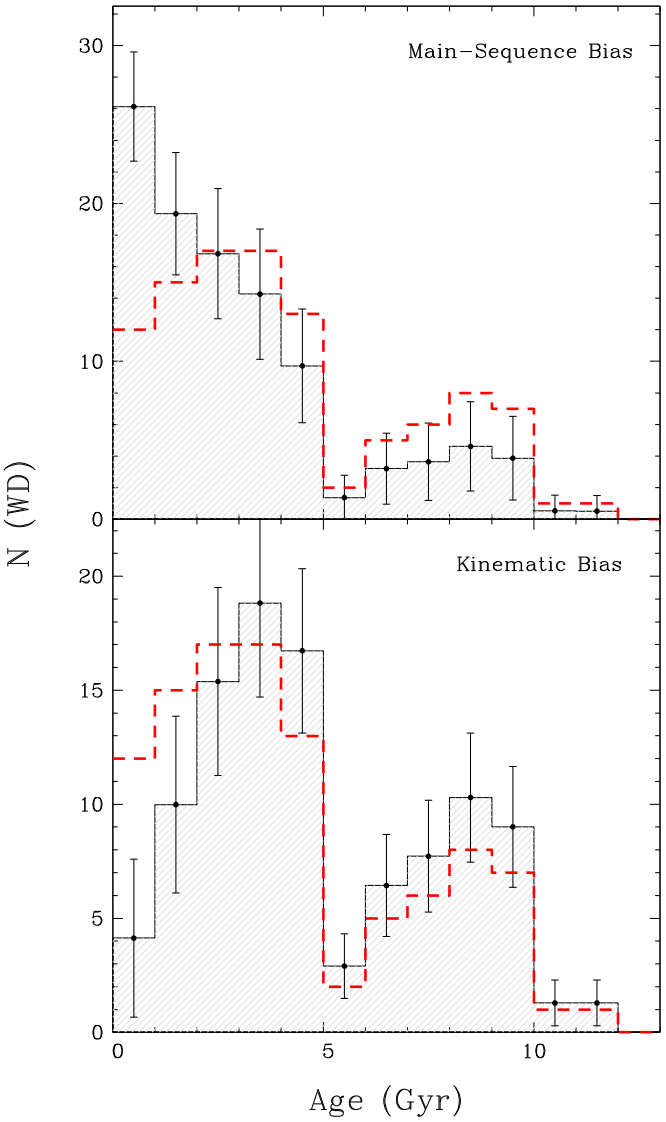

Figure 4. Similar to Figure 3 with the raw data from Figure 2 shown with a red dashed curve. The black filled histograms account for only one bias, due to missing main-sequence stars (top panel), and velocity dispersion (bottom panel), respectively. The distributions were re-normalized for the same total number of objects. The error bars take into account number statistics and are derived from the uncorrected number of white dwarfs.

(A color version of this figure is available in the online journal.)

using distances from GB12. While most objects are consistent with thin disk kinematics, it is difficult to disentangle thin versus thick disk populations even based on three-dimensional kinematics (Kawka & Vennes 2006; Sion et al. 2009). We note, however, the presence of a correlation between age and velocity, and in particular a significant $v_{\rm tan}$ increase in the range $9 < {\rm Age(Gyr)} < 11$, a population that represents about 8% of the sample. The derived total ages in this range are sensitive to the parameterization of the initial–final mass relation (see Section 4.1). Furthermore, three objects do not even have mass measurements. These objects are relatively old with a mean cooling age of 7.8 Gyr, assuming $\log g = 8.0$, hence they could be remnants of short-lived main-sequence stars, be closer, and have smaller velocities than assumed. Therefore, it is difficult to confirm the mean age of this population, and whether it represents the tail of the thin disk or a separate thick disk population. Sion et al. (2009) argue that there is no obvious

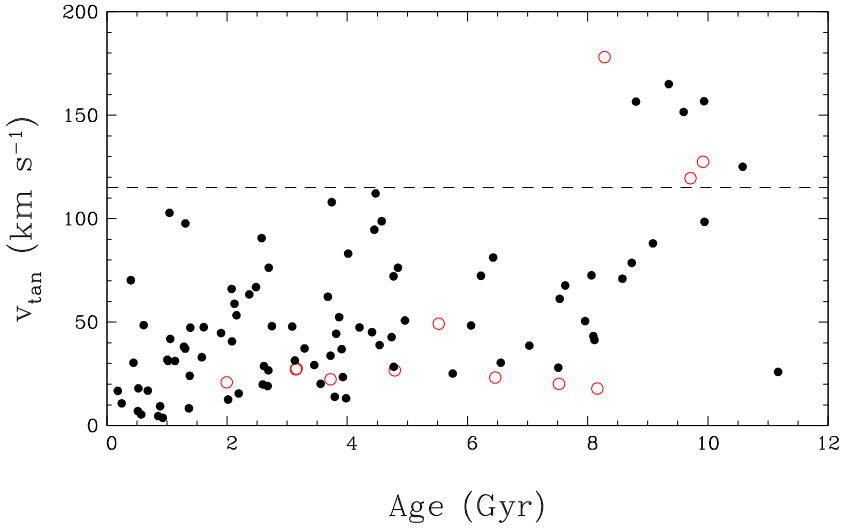

Figure 5. Tangential velocities for the white dwarfs in the local sample as a function of total age. v_{tan} was computed from the known distances (GB12) and proper motions (Sion et al. 2014). Remnants with a fixed $\log g = 8.0$ value are identified with open red circles.

(A color version of this figure is available in the online journal.)

separation between the thin and thick disk populations in the 20 pc sample, an interpretation that is in agreement with the review of the stellar content of the SDSS SEGUE survey showing no distinct thick disk component in our Galaxy (Bovy et al. 2012). On the other hand, the UVW three-dimensional space motions of the white dwarfs in the SN Ia Progenitor survey (SPY; Pauli et al. 2006) revealed that 7% of their sample belongs to the thick disk, in agreement with the local sample at face value. Reid (2005) suggests a thick disk population of as much as 20% in the solar neighborhood, which could still be compatible with the local sample considering that high-velocity components are under represented in a volume-complete sample.

The population identification for the local sample is not essential for our study as long as one keeps in mind that the derived SFH might not exclusively account for the thin disk. More critical is the bias caused by changes in the dispersion of the vertical component of the velocity in Galactic coordinates (σ_W) as a function of age. We refrain from studying this issue directly from the local white dwarfs since the subsample having three-dimensional velocities is far from complete and not homogeneous. Instead we rely on the studies of Nordström et al. (2004) and Seabroke & Gilmore (2007) who determined σ_W versus age for a large sample of nearby F and G stars. Both studies agree that σ_W increases by a factor of two in the 1–5 Gyr age range. Seabroke & Gilmore (2007) propose a new binning procedure and suggest the relation

$$\sigma_W = k\mathrm{age}^{0.6}, \quad (3)$$

where k is a constant. They demonstrate that it is unclear whether this trend continues for ages larger than 5 Gyr or if there is a saturation at constant σ_W for thin disk stars. We consider the latter possibility as our standard correction, but review the former possibility in Section 4.1. The volume bias correction is at first order directly proportional to σ_W and is shown in Figure 4 (bottom panel) compared to the raw data. This correction has a slope, as a function of age, with an opposite sign compared to the missing main-sequence star bias described in the previous section, hence the effects largely cancel each other out in our resulting best estimate of the SFH in Figure 3.

4. DISCUSSION

4.1. Assessing Biases

We review in turn the different biases and uncertainties in our best estimate of the SFH presented in Figure 3. Several experiments are presented in Figures 6 and 7 and described in this section. First of all, in Figure 6, we use a steeper theoretical power-law for the IMF, with an index of −3.2 instead of the commonly used Salpeter law with a slope of −2.35 as a function of increasing $\log M_\odot$. The steeper IMF is closer to the observed value for the local sample. The impact is mostly seen for the first age bin, where the bias correction for the ratio between white dwarfs and stars is critical. This demonstrates that due to the uncertain IMF, we cannot constrain very well the slope of the SFH in the last 3 Gyr, although this does not change much the overall shape of the SFH. We have also used an alternative description of the σ_W versus age relation, by relying on Equation (3) at all ages, which is more consistent with the interpretation of Nordström et al. (2004). It increases the bias correction for old white dwarfs in Figure 6, although the overall shape of the SFH is similar.

The following experiment in Figure 6 (bottom panel) employs the Catalán et al. (2008) initial–final mass relation instead of that of Kalirai et al. (2008). These studies were the first to put significant constraints on the low-mass end of the relation, the former by examining white dwarfs in common proper motion pairs. The results demonstrate that total age uncertainties are of the order of 1 Gyr since a significant amount of white dwarfs are shifted to the next bin. There are more objects with a total age older than 10 Gyr when using the Catalán et al. relation. This confirms the difficulty of assigning a population membership to the oldest white dwarfs in the local sample, although the overall shape of the SFH does not depend appreciably on the initial–final mass relation. Finally, the last experiment in Figure 6 takes the alternative white dwarf cooling sequences of Salaris et al. (2010) as input for the total age. We rely on the sequences including the effects of C/O phase separation and sedimentation in the core. Since radii were not available in their table, we still used the mass–radius relation of Fontaine et al. (2001). Nevertheless, it illustrates that differences in the independent cooling models do not have a significant impact on our results.

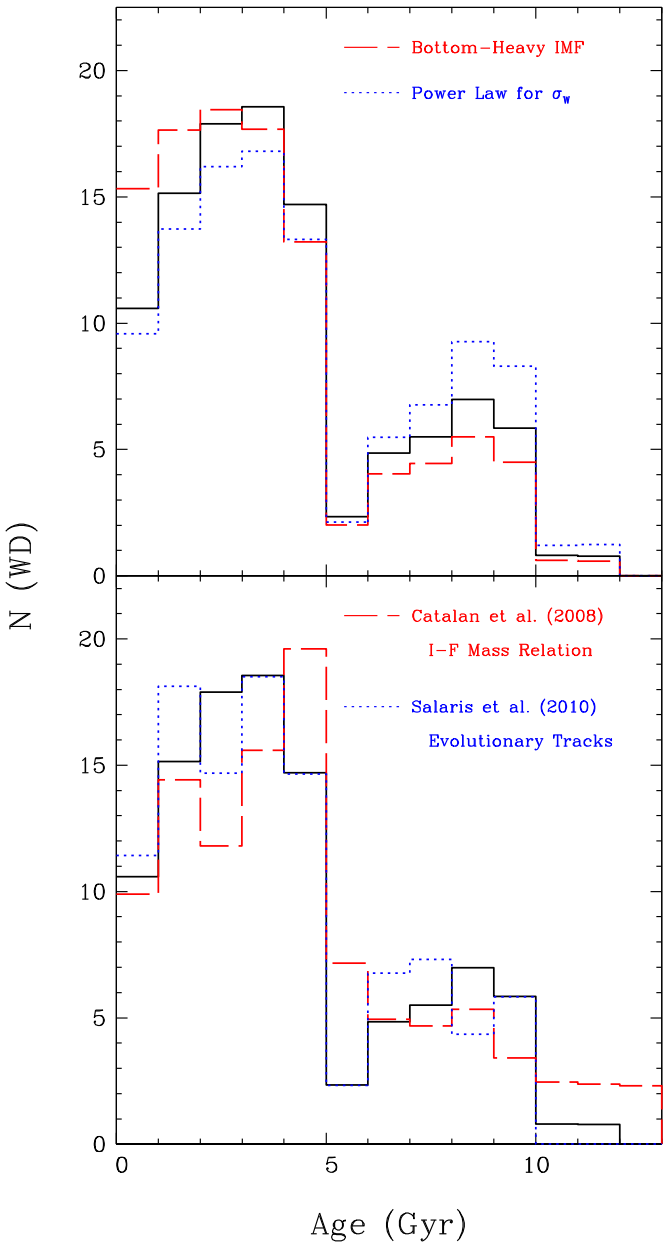

Figure 6. Alternative derivations of the SFH compared to our best standard estimate of Figure 3 (solid black curves). All distributions were re-normalized to have the same total number of objects. Top panel: we rely on a steeper power law IMF with an index of −3.2 instead of −2.35 for the standard Salpeter case (dashed red). We use the power law of Equation (3) for the σ_W vs. age relation at all ages (dotted blue) instead of assuming a saturation above 5 Gyr. Bottom panel: we employ the initial–final mass relation of Catalán et al. (2008; dashed red) instead of the one from Kalirai et al. (2008). Finally, we take the Salaris et al. (2010) cooling tracks (dotted blue) instead of those from Fontaine et al. (2001).

(A color version of this figure is available in the online journal.)

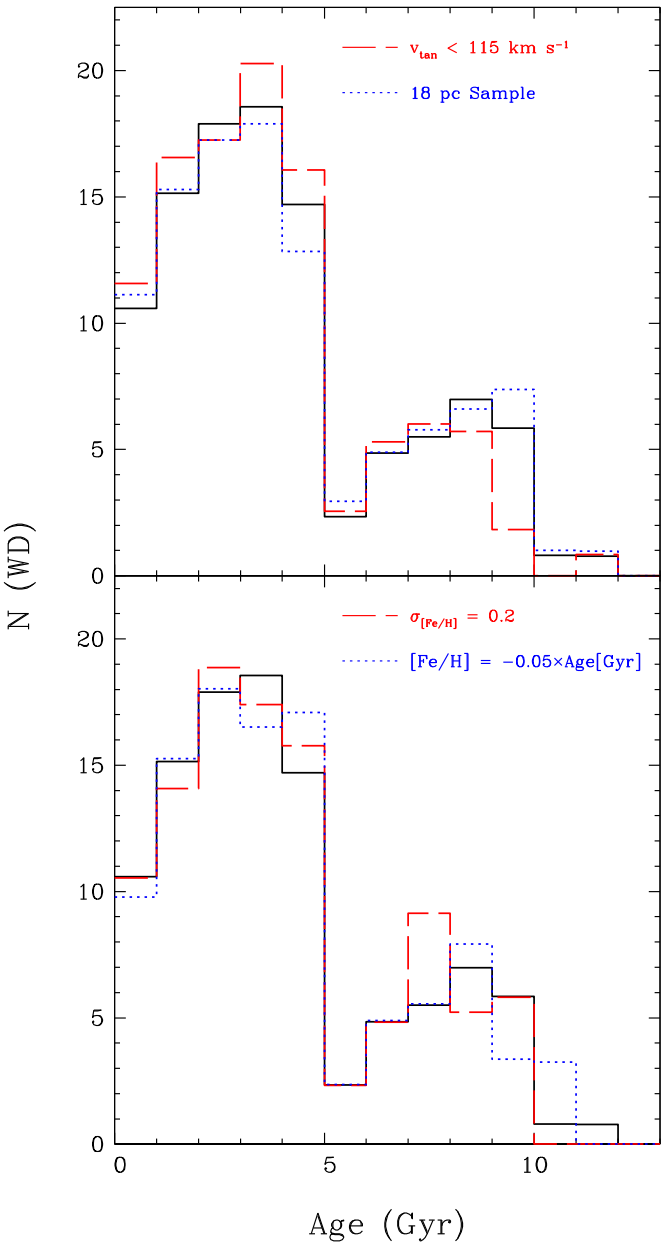

Figure 7. Similar to Figure 6 but with additional alternative derivations of the SFH. All distributions are re-normalized to the same integrated number of stars. Top panel: the high velocity population ($v_{\rm tan} > 115$ km s^{-1}) is removed (dashed red), and the more complete 18 pc sample is used instead of the standard 20 pc sample (dotted blue). Bottom panel: the main-sequence lifetimes are computed with metallicities derived from a Monte Carlo simulation with a dispersion of $\sigma_{\rm [Fe/H]} = 0.2$ around solar metallicity (dashed red), or a linear age vs. metallicity relation with a solar value at present time and a value of [Fe/H] = −0.5 at 10 Gyr (dotted blue).

(A color version of this figure is available in the online journal.)

The second series of experiments in Figure 7 starts with a tangential velocity cutoff in order to remove a population that is potentially not part of the thin disk. We made the cutoff at $v_{\rm tan} < 115$ km s^{-1} based on the results of Figure 5. While there is a more rapid dip in the SFH for ages larger than 9 Gyr, the overall shape at earlier ages is unchanged. Another uncertainty comes from the incompleteness of the sample as well as the incomplete information for 12 objects with no log g determinations. Since the latter objects are mostly cool white dwarfs with no or weak spectral features, they are unambiguously old and it is unlikely that log g determinations, even if the mean value was significantly different to 8.0, would change the SFH picture. We estimated in Section 2 that the sample is 82% complete. To illustrate the impact of this bias, we rely instead on the 18 pc sample, which is expected to be 92% complete, to derive the SFH in Figure 7. The effect is relatively mild, and there is no clear age dependence as one could have expected since missing white dwarfs are more likely to be fainter than the average. However, this does not necessarily imply very old ages for the faintest remnants, since a white dwarf with a 2 Gyr cooling time

already has a temperature of ∼6000 K, which is not far from the coolest objects in the sample ($T_{\rm eff} \sim 4000$ K).

The last uncertainty that we discuss in this section is the assumption that all stars were formed with a solar metallicity. This is based on the fact that we cannot recover the initial metallicity from white dwarf observations. The age versus metallicity relation is not very well understood (Soderblom 2010). It impacts first of all the total main-sequence lifetime, and there are indications it may also impact the initial–final mass relations (Zhao et al. 2012), although we already accounted for this uncertainty above by looking at two different relations calibrated from different populations (and metallicities). We made a Monte Carlo experiment in which the initial metallicities for the local sample were randomly selected from a normal distribution with a dispersion of [Fe/H] = 0.2 and a mean solar value. This supposition corresponds for instance to the observations of Fuhrmann (1998) for FGK stars in the solar neighborhood. In a second experiment, we assume a simple linear age versus metallicity relation with a solar value at present time, and a subsolar [Fe/H] = −0.5 metallicity at 10 Gyr. Figure 7 (bottom panel) demonstrates that the impact is relatively small on the SFH with both assumptions. The total age does not strongly depend on the metallicity, and there is no systematic offset with a linear metallicity variation as a function of age. This is because the large age bins are populated with objects having both short and long main-sequence lifetimes, for high and low mass white dwarfs, respectively.

We conclude that the two-step feature of the SFH, with an enhanced formation rate in the last 5 Gyr compared to the range 5 < Age(Gyr) < 10, is a significant detection for the 20 pc sample. The total number of stars formed more than 5 Gyr ago is 30, versus 74 objects at a younger age, which is a 3σ result unlikely to be compromised by biases. On the other hand, smaller scale fluctuations are unlikely to be significant. The small size of the sample is the primary uncertainty in the overall derivation of the SFH, given the error bars in Figure 3. The most important additional uncertainty in the lower age bins is the IMF in the solar neighborhood. Different uncertainties come into play for the oldest remnants, including the uncertain low-mass end of the initial–final mass relation, the separation between thin and thick disk populations, and the bias from the velocity dispersion versus age relation. Furthermore, the age of old white dwarfs is uncertain by ∼1 Gyr because of the elusive C/O ratio in the core (see Figure 7 of Fontaine et al. 2001). However, it is fairly evident that the oldest white dwarfs in the solar neighborhood have an age of at least 8 Gyr due to their unambiguous cool temperatures and cooling times.

4.2. Comparison with other Studies

In principle, our study is most easily compared to the derivation of the SFH from white dwarf luminosity functions. The main difference compared to our direct technique is that the information about individual masses and total ages is lost in the luminosity function. In order to compare these independent techniques, we performed Monte Carlo simulations for a volume complete 100 pc sample using the total space density from GB12. We suppose a Salpeter IMF while main-sequence lifetimes, cooling sequences, the velocity dispersion versus age relation, and the initial–final mass relation are based on the same models as those described in Section 3. The simulated luminosity functions presented in Figure 8 either assume our derived SFH of Figure 3 (filled points) or a constant SFH in the last 10 Gyr (open points). The results suggest that

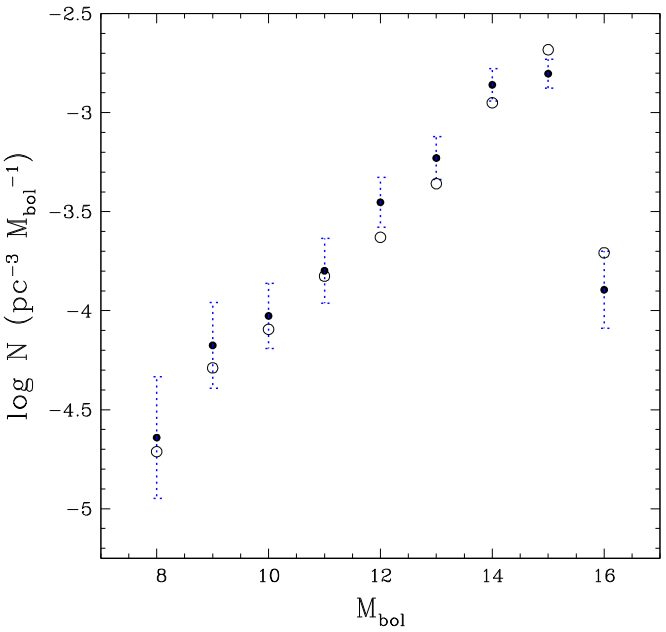

Figure 8. Simulated white dwarf luminosity functions for a 100 pc volume complete sample assuming our derived SFH for the local sample (solid circles), or a constant SFH for the last 10 Gyr (open circles). In both cases, the space density of white dwarfs is fixed at 4.39×10^{-3} pc^{-3} (GB12). We rely on the main-sequence lifetimes of Hurley et al. (2000), the initial–final mass relation of Kalirai et al. (2008), the cooling sequences of Fontaine et al. (2001), the velocity dispersion vs. age relation of Equation (3) (below 5 Gyr), and suppose a Salpeter IMF. We also present the error bars (blue, dotted) from the number statistics of the local 20 pc sample.

(A color version of this figure is available in the online journal.)

the luminosity function has a signature of a non-constant SFH. Figure 8 also shows the error bars based on number statistics for the 20 pc sample, illustrating that a larger volume complete sample is necessary to extract a statistically significant SFH from the luminosity function. As a consequence, we make no attempt to model the observed luminosity function of GB12. Furthermore, there is no guarantee that the observed luminosity function defines an unique solution for the SFH.

Rowell (2013) derived the SFH from the inversion of the white dwarf luminosity functions in the SDSS (Harris et al. 2006) and the SuperCOSMOS Sky Survey (Rowell & Hambly 2011). One advantage is that their observed samples are significantly larger than the local sample. As we did in this work, they reviewed the different biases impacting their results, and similarly determined that the initial–final mass relation, IMF, and initial metallicity have little influence on the SFH. However, they obtained that the cooling models have a strong impact on the SFH, an interpretation that we do not support. We suggest instead that the different cooling sequences highlight a shortcoming in the inversion technique or the bias corrections for the incompleteness of the samples. We refrain from a qualitative comparison with the results of Rowell (2013) until these issues are resolved, although we notice that they observe bimodal distributions for both samples they studied, with a stellar formation minimum at ∼5 Gyr, which is in agreement with our study. They have significant formation peaks at older ages, between 7 and 10 Gyr, which is not supported at face value by our study, even though our experiment with a high velocity dispersion for old objects in Figure 6 supports a smaller second peak.

There are many local SFH studies based on stellar observations, using rather different techniques. None of them are a direct

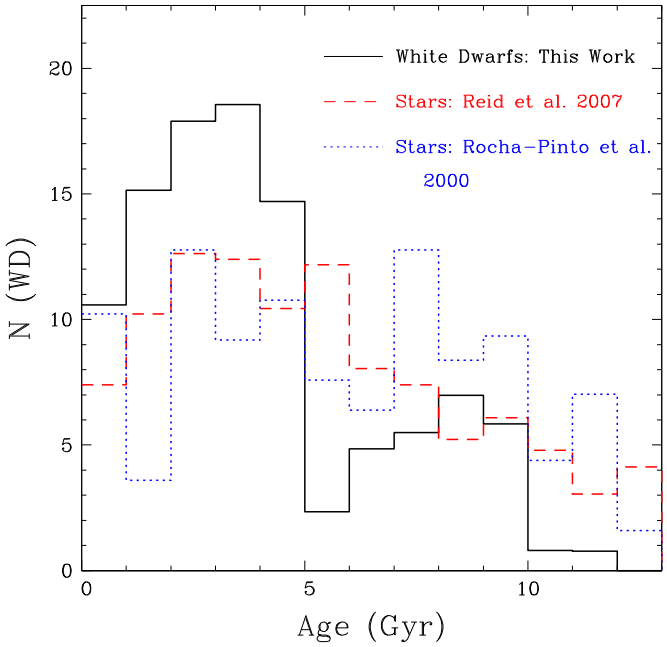

Figure 9. Comparison of our derived SFH (solid black) with the studies of Reid et al. (2007; Sample A, dashed red) and Rocha-Pinto et al. (2000; dotted blue) based on the age vs. metallicity distribution of Valenti & Fischer (2005), and chromospheric ages, respectively. The stellar distributions are re-binned and re-normalized to the white dwarf distribution.

(A color version of this figure is available in the online journal.)

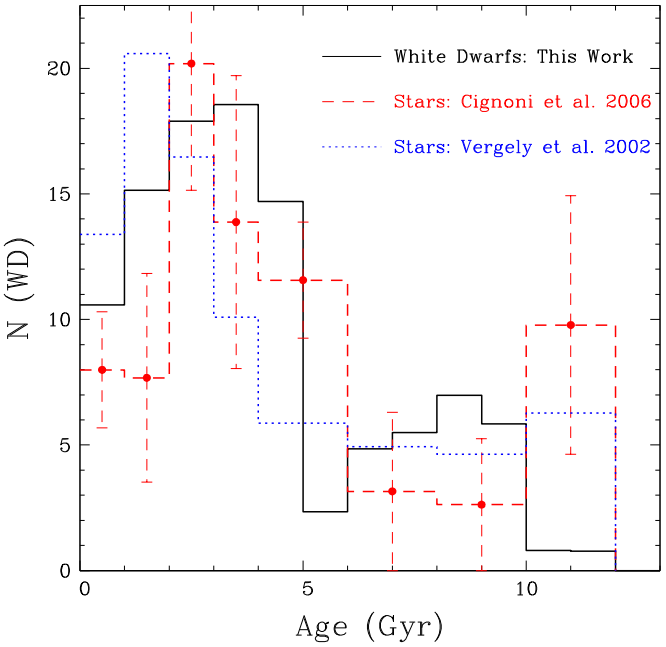

Figure 10. Comparison of our derived SFH (solid black) with the studies of Cignoni et al. (2006; dashed red) and Vergely et al. (2002; dotted blue) based on the inversion of the observed *Hipparcos* color–magnitude diagram in the solar neighborhood. The stellar distributions are re-normalized to the white dwarf distribution. We also add the uncertainties given in Cignoni et al. (2006) as an illustrative example of the errors.

(A color version of this figure is available in the online journal.)

equivalent to our technique since ages are typically not available for all stars in volume-complete samples. Reid et al. (2007) relied on a nearly complete sample of ∼500 stars identified from *Hipparcos* with absolute magnitudes $4 < M_V < 6$ within 30 pc. About half of the stars are also part of the Valenti & Fischer (2005) sample of high-resolution echelle spectra from which they determined precise atmospheric parameters and thereafter derived ages from stellar isochrones. Reid et al. (2007) used the age versus metallicity relation from this subsample to estimate ages for the other half of the sample, where metallicities were derived from the Strömgren colors. This technique is not without problems since there is a significant scatter in the age versus metallicity relation and ages well over 15 Gyr are found for many stars in the sample. In Figure 9, we compare our results to those of Reid et al. (2007, Sample A), showing that their roughly constant SFH is not compatible with our findings.

A second group of studies also relies on *Hipparcos* data of F and G stars to place them on color–magnitude diagrams. Instead of assigning individual ages, they rely on Bayesian techniques to invert the observed color–magnitude diagram into an SFH. Much like the study of Reid et al. (2007), a set of stellar isochrones is at the center of age determinations. The analysis of Vergely et al. (2002) constrains simultaneously the SFH and age versus metallicity relation, as well as the IMF and SFH in a separate experiment. Furthermore, they do not limit the distance in the vertical Galactic coordinate ensuring they are not biased against velocity dispersion. On the other hand, Cignoni et al. (2006) rely on a hybrid approach, also inverting the color–magnitude diagram but using underlying assumptions for the IMF and age versus metallicity relation. They employ a volume complete *Hipparcos* sample with $M_V < 3.5$ and distances within 80 pc. They demonstrate that the recovered SFH is not very sensitive to the assumed IMF, binary fraction, possible stellar streams, and velocity cuts. However, they find that the age versus metallicity relation has a significant impact on the outcome, and in spite of that, adopt a constant metallicity versus age relation with a scatter of $\sigma_{[Fe/H]} = 0.2$ to match the observations of Nordström et al. (2004). The utilization of a different relation, such as the linear relation employed by Reid et al. (2007), would have resulted in an appreciably different SFH (see Figure 9 of Cignoni et al.). In addition, they suggest that their SFH is significantly undersampled for ages larger than 7 Gyr due to the lack of good age tracers with $M_V < 3.5$. Figure 10 compares our findings with those of Vergely et al. (2002) and Cignoni et al. (2006), showing this time a relatively good agreement. As an illustration, we also add the error bars derived by Cignoni et al. (2006), demonstrating that even though we have a much smaller number of objects in our sample in Figure 3, our error bars are not remarkably larger. All of the stellar studies described above are also subject to uncertainties in the predicted isochrones, which are difficult to constrain and not typically included in the quoted uncertainties (Soderblom 2010).

Most other techniques employed to derive the SFH are limited to small lookback times (de la Fuente Marcos & de la Fuente Marcos 2004; Fuchs et al. 2009), but support the view of Vergely et al. (2002) and Cignoni et al. (2006) about a formation peak a few Gyr ago. However, Rocha-Pinto et al. (2000) studied the chromospheric age distribution of 552 late-type dwarfs and converted their results to a SFH by applying scale height, volume, and stellar evolution corrections. We present their results in Figure 9 where the SFH is roughly constant with age, once again in opposition to our results. While chromospheric age determination is in principle straightforward and provides ages with a precision of ∼0.2 dex (Soderblom et al. 1991), the interpretation at young ages differs between studies (Fuchs et al. 2009) and activity can be difficult to detect in older stars.

All in all, the comparison of our results with stellar studies is difficult because of the conflicting derived SFH ranging from constant values in Figure 9 to peaked distributions at young ages

in Figure 10. Our white dwarf derived SFH is in better overall agreement with the studies of Vergely et al. (2002) and Cignoni et al. (2006), although this does not necessarily support their techniques over others since the agreement is only qualitative. There is a similarity over the notable drop in the stellar formation for ages older than ∼5 Gyr and younger than 10 Gyr. Vergely et al. (2002) and Cignoni et al. (2006) predict this transition at younger and older ages than our study, respectively. For ages larger than 10 Gyr, both stellar studies predict a significant number of stars although Cignoni et al. (2006) are cautious and attribute their second peak to undersampling. In our case, the lack of stars older than 10 Gyr is consistent with the derived age of the disk from white dwarfs (Leggett et al. 1998), which is not entirely surprising since the early studies looking at the age of remnants used some of the objects and observations from the current local sample.

Due to the intrinsic brightness of the FGK stars, stellar studies typically cover a significantly larger volume than our white dwarf sample. However, it does not necessarily imply lower error bars on the SFH since uncertainties for individual ages are large for stars. One advantage of the stellar studies is that they have a better sampling of the vertical scale height of the disk. Faint stellar streams that are observed in the solar neighborhood (Seabroke & Gilmore 2007) may impact the derived SFH, especially for smaller samples, and our derived SFH within 20 pc may not represent that of the Galactic disk. Nevertheless, the fact that we recover the results of Vergely et al. (2002) and Cignoni et al. (2006) suggests that streams are not an issue.

5. CONCLUSION

We presented a new technique where individual white dwarf atmospheric parameters, for a volume complete sample, are used to derive the SFH in the solar neighborhood. The method compares advantageously to other techniques aimed at extracting the SFH for the Galactic disk. The success of the method resides in the fact that the white dwarf masses and cooling ages, the main-sequence lifetime as a function of mass, and the initial–final mass relation are all relatively well constrained quantities. Therefore, it allows for a precise transformation of the remnant atmospheric parameters to total ages and initial masses. The main uncertainties for the age of old remnants are the scatter in the observed initial–final relation and the well-known unconstrained composition of the core (Fontaine et al. 2001). We found that it is also difficult to identify the thin or thick disk nature of the old remnants, although it does not impact significantly our derivation of the overall SFH. At very young ages, the main shortcoming is the lack of stars that became white dwarfs. Finally, the largest limitation of the current analysis is the small size of the 20 pc sample. However, future surveys like *Gaia* will resolve this issue.

The SFH derived from white dwarfs was compared to similar studies relying on large samples of FGK stars and the chromospheric activity in late-type dwarfs. There are conflicting results in these studies, and we suggest that the SFH from white dwarfs may be the most accurate at intermediate and large ages. We recover a significant enhanced formation rate in the last ∼5 Gyr by a factor ∼2.5 of compared to the range 5–10 Gyr. This result is in agreement with a number of studies looking at the stellar content of the solar neighborhood.

Support for this work was provided by NASA through Hubble Fellowship grant HF-51329.01 awarded by the Space Telescope Science Institute, which is operated by the Association of Universities for Research in Astronomy, Inc., for NASA, under contract NAS 5-26555. This project was supported by the National Science Foundation (NSF) through grant AST-1211719.

REFERENCES

Bergeron, P., Saffer, R. A., & Liebert, J. 1992, ApJ, 394, 228
Bergeron, P., Wesemael, F., Dufour, P., et al. 2011, ApJ, 737, 28
Bovy, J., Rix, H.-W., & Hogg, D. W. 2012, ApJ, 751, 131
Brown, J. M., Kilic, M., Brown, W. R., & Kenyon, S. J. 2011, ApJ, 730, 67
Carrasco, J. M., Catalán, S., Jordi, C., et al. 2014, A&A, 565, A11
Catalán, S., Isern, J., García-Berro, E., & Ribas, I. 2008, MNRAS, 387, 1693
Cignoni, M., Degl'Innocenti, S., Prada Moroni, P. G., & Shore, S. N. 2006, A&A, 459, 783
de la Fuente Marcos, R., & de la Fuente Marcos, C. 2004, NewA, 9, 475
Diaz-Pinto, A., Garcia-Berro, E., Hernanz, M., Isern, J., & Mochkovitch, R. 1994, A&A, 282, 86
Dobbie, P. D., Day-Jones, A., Williams, K. A., et al. 2012, MNRAS, 423, 2815
Dufour, P., Bergeron, P., & Fontaine, G. 2005, ApJ, 627, 404
Dufour, P., Bergeron, P., Liebert, J., et al. 2007, ApJ, 663, 1291
Fontaine, G., Brassard, P., & Bergeron, P. 2001, PASP, 113, 409
Fuchs, B., Jahreiß, H., & Flynn, C. 2009, AJ, 137, 266
Fuhrmann, K. 1998, A&A, 338, 161
Giammichele, N., Bergeron, P., & Dufour, P. 2012, ApJS, 199, 29
Harris, H. C., Munn, J. A., Kilic, M., et al. 2006, AJ, 131, 571
Hernandez, X., Valls-Gabaud, D., & Gilmore, G. 2000, MNRAS, 316, 605
Holberg, J. B., Oswalt, T. D., & Sion, E. M. 2002, ApJ, 571, 512
Holberg, J. B., Oswalt, T. D., Sion, E. M., Barstow, M. A., & Burleigh, M. R. 2013, MNRAS, 435, 2077
Holberg, J. B., Sion, E. M., Oswalt, T., et al. 2008, AJ, 135, 1225
Hurley, J. R., Pols, O. R., & Tout, C. A. 2000, MNRAS, 315, 543
Kalirai, J. S., Hansen, B. M. S., Kelson, D. D., et al. 2008, ApJ, 676, 594
Kalirai, J. S., Richer, H. B., Reitzel, D., et al. 2005, ApJL, 618, L123
Kalirai, J. S., Saul Davis, D., Richer, H. B., et al. 2009, ApJ, 705, 408
Kawka, A., & Vennes, S. 2006, ApJ, 643, 402
Kowalski, P. M., & Saumon, D. 2006, ApJL, 651, L137
Leggett, S. K., Ruiz, M. T., & Bergeron, P. 1998, ApJ, 497, 294
Liebert, J., Bergeron, P., & Holberg, J. B. 2005, ApJS, 156, 47
Liebert, J., Dahn, C. C., & Monet, D. G. 1988, ApJ, 332, 891
Limoges, M.-M., & Bergeron, P. 2010, ApJ, 714, 1037
Nordström, B., Mayor, M., Andersen, J., et al. 2004, A&A, 418, 989
Pauli, E.-M., Napiwotzki, R., Heber, U., Altmann, M., & Odenkirchen, M. 2006, A&A, 447, 173
Reid, I. N. 2005, ARA&A, 43, 247
Reid, I. N., Turner, E. L., Turnbull, M. C., Mountain, M., & Valenti, J. A. 2007, ApJ, 665, 767
Rocha-Pinto, H. J., Scalo, J., Maciel, W. J., & Flynn, C. 2000, A&A, 358, 869
Rowell, N. 2013, MNRAS, 434, 1549
Rowell, N., & Hambly, N. C. 2011, MNRAS, 417, 93
Salaris, M., Cassisi, S., Pietrinferni, A., Kowalski, P. M., & Isern, J. 2010, ApJ, 716, 1241
Salpeter, E. E. 1955, ApJ, 121, 161
Seabroke, G. M., & Gilmore, G. 2007, MNRAS, 380, 1348
Sion, E. M., Holberg, J. B., Oswalt, T. D., et al. 2014, AJ, 147, 129
Sion, E. M., Holberg, J. B., Oswalt, T. D., McCook, G. P., & Wasatonic, R. 2009, AJ, 138, 1681
Soderblom, D. R. 2010, ARA&A, 48, 581
Soderblom, D. R., Duncan, D. K., & Johnson, D. R. H. 1991, ApJ, 375, 722
Tremblay, P.-E., Bergeron, P., & Gianninas, A. 2011, ApJ, 730, 128
Tremblay, P.-E., Ludwig, H.-G., Steffen, M., & Freytag, B. 2013, A&A, 559, A104
Tremblay, P.-E., Schilbach, E., Röser, S., et al. 2012, A&A, 547, A99
Valenti, J. A., & Fischer, D. A. 2005, ApJS, 159, 141
Vergely, J.-L., Köppen, J., Egret, D., & Bienaymé, O. 2002, A&A, 390, 917
Weisz, D. R., Fouesneau, M., Hogg, D. W., et al. 2013, ApJ, 762, 123
Williams, K. A. 2004, ApJ, 601, 1067
Williams, K. A., Bolte, M., & Koester, D. 2009, ApJ, 693, 355
Winget, D. E., Hansen, C. J., Liebert, J., et al. 1987, ApJL, 315, L77
Zhao, J. K., Oswalt, T. D., Willson, L. A., Wang, Q., & Zhao, G. 2012, ApJ, 746, 144